した.

4．出力は，フィルム出力とし，ディジタルデータを自動現像機(CR = LPD, FUJI FILM MEDICAL)に転送し，半切サイズ(LILM)にて行った.

3.2 観察者

観察者は，経験年数10年，18年，20年の愛媛大学医学部放射線医学教室の胸部グループ放射線科医3名とした.

3.3 ROC評価

1．試料数は信号あり40枚，信号なし40枚，それぞれの胸部画像，軟部組織画像80枚の計160枚とした.

2．観察者は，あらかじめどの様な陰影が存在するか学習し，通常の胸部画像の読影を行い，専用用紙(1試料1枚)に確信度を記載した．読影後，補助者が専用用紙に試料番号を記入した.

3．観察距離は通常の読影作業と同じくシャーカステンから約50cmとした.

4．観察時間は1試料あたり60秒とした.

5．信号有り40枚，信号無し40枚計80枚の胸部画像は，すべて試料番号を付け，読影画像順位は試料提示者が無作為に抽出した.

6．2週間の期間をあけ，再度同一観察者が読影をおこない，胸部画像と軟部組織画像の2枚の画像を読影後，確信度を記載し，前回同様補助者が試料番号を解答用紙に記載した.(試料番号記載は，結果判定に必要)

3.4 ROC評価結果算出

1．解答用紙の確信度を数値化し，各読影者ごとにコンピュータに入力し計算させた．使用ソフトは，シカゴ大学カートロスマン放射線像研究所メッツ教授の御厚意によりインストールしたROCKITを使用した.

2．得られた結果をエクセルにて数値化し，ROC曲線を得た.

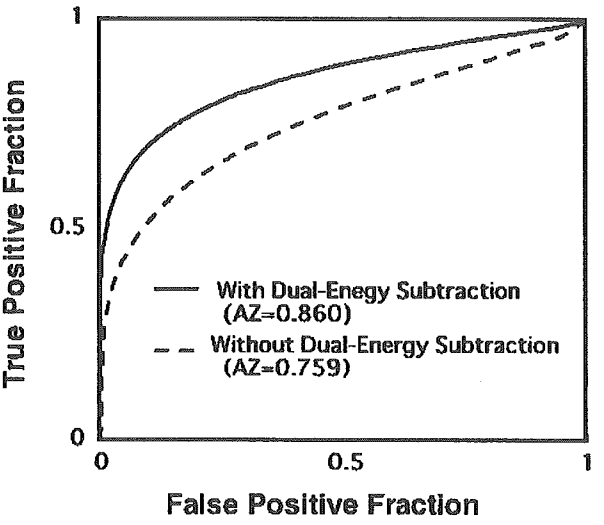

Fig. 4 ROC CURVE of nodule(10y) With Dual-Energy Subtraction (AZ = 0.860) Without Dual-Energy Subtraction(AZ=0.759)

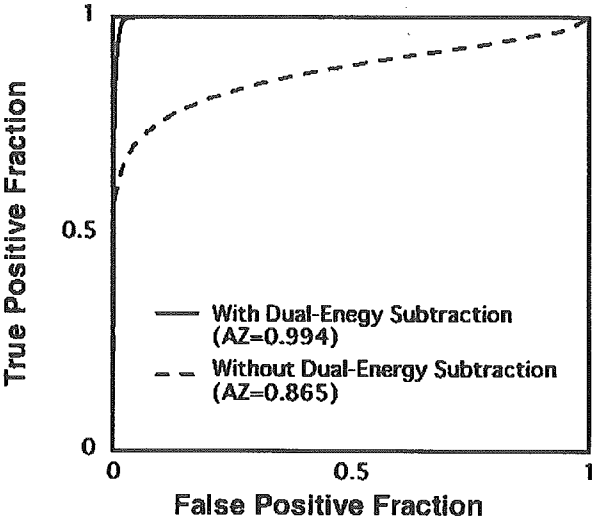

Fig. 5 ROC CURVE of nodule(18y) With Dual-Energy Subtraction (AZ = 0.994) Without Dual-Energy Subtraction(AZ=0.865)

4. 結　果

胸部放射線科医の読影結果を基に作成したROC曲線を示す(Fig. 4−7)．経験10年の放射線科医の評価結果をFig. 4に示す．AZ値が0.759から0.860と改善されており，軟部組織画像を用いる事により検出能の向上が認められた．次に経験18年の放射線科医の評価結果をFig. 5に示す．前者同様．AZ

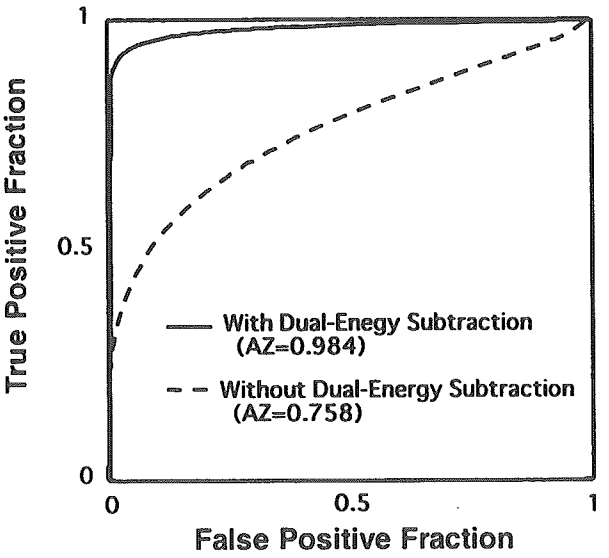

Fig. 6 ROC CURVE of nodule(20y)With Dual-Energy Subtraction (AZ = 0.984) Without Dual-Energy Subtraction(AZ=0.758)

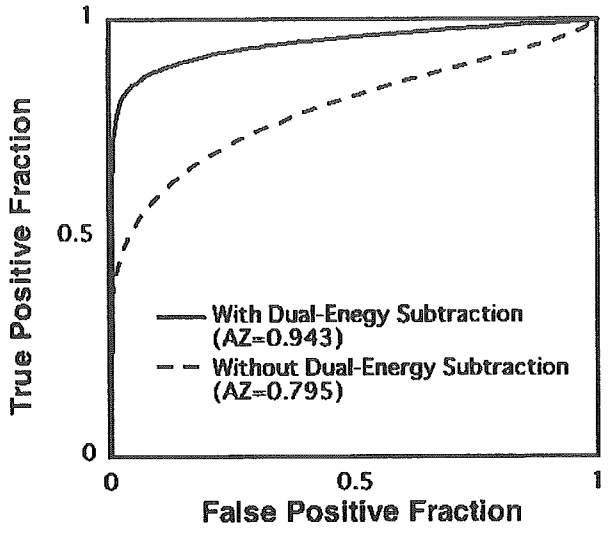

Fig. 7 ROC CURVE of nodule(Over all)With Dual-Energy Subtraction (AZ=0.943)Without Dual-Energy Subtraction(AZ=0.795)

値が0.865から0.994と改善されており，軟部組織画像を用いる事により検出能の向上が認められた．

経験20年の放射線科医の評価結果をFig. 6に示す．本結果も前者同様，AZ値が0.758から0.994と改善されており，軟部組織画像を用いる事により検出能の向上が認められた．胸部グループ放射線科医3名の平均をFig. 7に示す．平均結果もAZ値が0.795から0.943と改善されており，軟部組織画像を用いる事により検出能の向上が認められた．

以上の結果，全てにおいて5%の危険率で2者間に有意差有りの検定結果となった．また今回，TWO SHOT法によるデュアルエネルギーサブトラクションを用いる事により，胸部腫瘤陰影の検出能の向上が認められた．

6. 考　察

現在，胸部異常陰影検出のためのスクリーニングとして，広く用いられる胸部単純画像は，その中に多くの情報があるにもかかわらず，その情報を取り出すには長い読影経験が必要となる．近年，その経験不足をおぎなうことを目的として，様々なCAD技術が開発されてきた．デュアルエネルギーサブトラクション法もその1つである．

今回著者らは，TWO SHOT法によるデュアルエネルギーサブトラクション法の胸部腫瘤陰影の検出能向上の有無を，ROC評価法(連続確信度法)にて行った．読影結果からTWO SHOT法によるデュアルエネルギーサブトラクションを用いることにより，胸部腫瘤陰影の検出能の向上が認められた(Table 1)．

Table. 1 Comparison of AZ value between without energy subtraction and with energy subtraction

	Dr.A(10y)	Dr.B(18y)	Dr.C(20y)	Over ALL
without energy subtraction(AZ)	0.759	0.866	0.758	0.795
with energy subtraction(AZ)	0.86	0.994	0.984	0.943

この原因としては，連続確信度法においてFalse NegativeからTrue Positiveへの移行，True Positiveの確信度(数値)の増加，False PositiveからTrue Negativeへの移行，True Negativeの確信度(数値)の減少が考えられる．

今回の実験から，TWO SHOT法によるデュアルエネルギーサブトラクションを用いることにより胸部異常陰影(ノジュール)の検出能向上が示唆された．

また，TWO SHOT法によるデュアルエネルギーサブトラクションでは，One Shot法に比べ粒状性の向上から，すりガラス状陰影(GGO)や網状陰影等

の検出能の向上も期待できる．

現在，同じシステムを標準で装備しているRevolution X R/dにて実際に臨床画像を収集しており，今後実際の臨床データの読影にてROC評価を行う予定である．また，One Shot法との比較も行ってみたい．

7．臨床データの紹介

参考までに興味深いいくつか臨床データを紹介する．

1．肋骨骨折(Fig. 8)

エネルギーサブトラクション処理により，肋骨の骨折部分がより鮮明に描出されている．

2．気管内異物(Fig. 9)

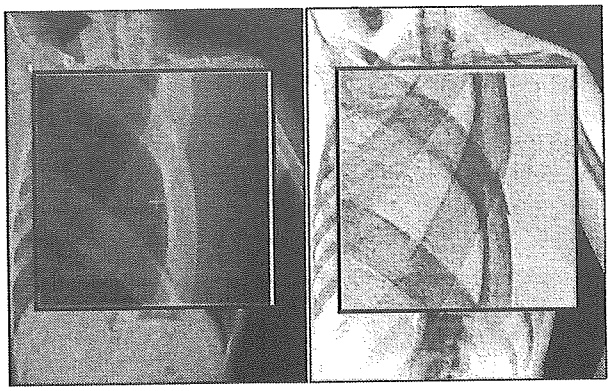

Fig. 8 Clinical Case1. Fracture of Rib

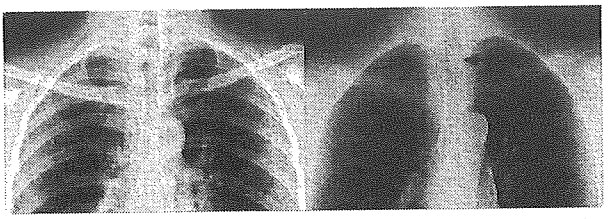

Fig. 9 Clinical Case2. Carcinoma of Inside of a tracheal gill

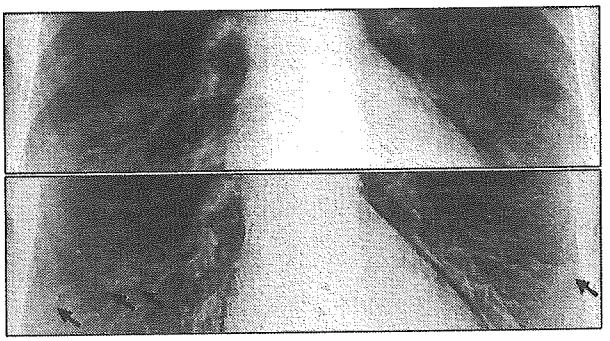

Fig. 10 Clinical Case3. Lung cancer(nodule)

胸部画像左は，通常より強い周波数処理を施しているにもかかわらず，気管内病変は検出できない．右は，軟部組織画像であるが，気管内の病変がよく観察できる．

3．腫瘤陰影(Fig. 10)

肋骨と重なって検出困難な症例である．軟部組織画像に数個腫瘤陰影が認められる．

8．謝　辞

今回の実験にあたり御助言頂いたシカゴ大学放射線像研究所　土井邦雄教授，白石順二先生，また読影に協力して頂いた愛媛大学医学部放射線医学教室の諸先生に深く感謝致します．

最後に，私にこの研究テーマを下さった，愛媛大学医学部放射線医学教室　故　池添潤平教授に感謝と哀悼の意を表します．

9．参考文献

[1] The Research Group for population-based Cancer Registration in Japan : Cancer incidence and Incidence Rates in Japan 1999 : Estimates Base on Date from 11 Population-based on Cancer Registries, Jpn, J. Clin.Oncol. , 34, 352-356, 2004.

[2] 長尾充展，久野梧郎，池添潤平，et al ：ヘリカルCTによる肺癌検診の初期成績，愛媛医学，18(4)，561-564, 1999.

[3] Kido S, Ikezoe J, Naito H,et al : Clinical evaluation of pulmonary nodules with single-exposure dual-energy subtraction chest radiography with an iterative noise-reduction algorithm, Radiology, 194(2)，407-412, 1995.

[4] Kido S, Kuriyama K, Hosomi N, et al : Low-cost soft-copy display accuracy in the detection of pulmonary nodules by single-exposure dual-energy subtraction : comparison with hard-copy viewing, J Digit Imaging, 13(1)，33-37, 2000.

[5] Wilkie JR, Giger ML, Chinander MR, et al : Investigation of physical image quality indices of

a bone densitometry system, Med. Phys, 31(4), 873-881, 2004.

[6] Kido S, Kuriyama K, Kuroda C, et al Detection of simulated pulmonary nodules by single-exposure dual-energy computed radiography of the chest : effect of a computer-aided diagnosis system(Part 2), Eur J Radiol., 44(3), 205-209, 2002.

[7] Kido S, Nakamura H, Ito W, et al : Computerized detection of pulmonary nodules by single-exposure dual-energy computed radiography of the chest(part 1). Eur J Radiol., 44(3), 198-204, 2002.

ORIGINAL ARTICLE

Radiation Medicine: Vol. 23 No. 6, 391–397 p.p., 2005

Clinical Evaluation of Pulmonary Nodules with Dual-exposure Dual-energy Subtraction Chest Radiography

Masahiko Uemura,[1] Masao Miyagawa,[1] Yoshifumi Yasuhara,[2] Tadashi Murakami,[1] Hirohiko Ikura,[1] Kana Sakamoto,[1] Hiroyuki Tagashira,[1] Kenji Arakawa,[1] and Teruhito Mochizuki[1]

Purpose: The purpose of this study was to assess the effect of dual-exposure dual-energy (DE) subtraction chest radiography with flat-panel detector.

Materials and Methods: One hundred patients underwent dual-exposure DE subtraction chest radiography and chest CT for evaluation of pulmonary nodules. Fifty-two patients with pulmonary nodules and 48 patients with normal lungs were selected for receiver operating characteristic (ROC) curve analysis. Ten radiologists who were unaware of the CT results evaluated chest radiography alone and chest radiography with DE subtraction images in the detection of pulmonary nodules. For each radiologist, we calculated the areas under the ROC curve (Az) for chest radiography alone and chest radiography with DE subtraction images.

Results: The average detectability of dual-exposure DE subtraction chest radiography was statistically significantly higher than that of chest radiography without subtraction images (mean Az value increased from 0.784 to 0.815, $p<0.001$).

Conclusion: Dual-exposure DE subtraction chest radiography improves diagnostic accuracy of pulmonary nodules.

Key words: diagnostic radiology, chest radiography, dual-energy subtraction, pulmonary nodule

Introduction

Chest radiography still represents the most common tool in diagnostic radiology due to its low cost, low dose, and simple implementation. However, it has been shown to have relatively low sensitivity for the detection of pulmonary nodules. Previous authors have indicated that overlying bone structures may obscure pulmonary lesions.[1,2] Dual-energy (DE) techniques are one of the possible methods to reduce anatomical noise. DE chest radiography involves taking an exposure of the patient using different energy x-ray beams. By exploiting the difference in the energy dependence of attenuation between bone and soft tissue, the contrast of the bone can be eliminated, producing a soft-tissue-only image, or the contrast of the soft tissue can be reduced to produce a bone image.[3]

Two approaches have been developed and evaluated by research groups: a single-exposure technique and a dual-exposure technique. In the single-exposure technique, one x-ray exposure is used to expose two stacked detectors that may be separated by a filter. The dual-exposure technique, such as that described in this study, employs two separate exposures: a high-energy exposure and a low-energy exposure that are subsequently applied to the same detector.[4] In previous studies, single-exposure DE techniques employing a storage phosphor system have proven advantageous in the detection of pulmonary nodules.[2,5-8] Despite these promising results, the single-exposure technique has not gained wide acceptance because of inconsistent image quality and difficulties in the handling and processing of images.[5,7]

Recently, full-field digital amorphous silicon flat-panel x-ray detector radiography systems based on cesium iodide (CsI) and amorphous silicon have become commercially available. These systems promise rapid access to the image for diagnosis, improved image quality relative to that of screen-film and storage phosphor systems, and possibilities for reduced radiation

Received January 5, 2005; revision accepted March 4, 2005.

[1]Department of Radiology, Ehime University School of Medicine
[2]Department of Radiology, Ehime National Hospital

Reprint requests to Masahiko Uemura, M.D., Department of Radiology, Ehime University School of Medicine, Shitsukawa, Toon, Ehime 791-0295, JAPAN.

exposure.[9] Development of a fast, high-efficiency flat-panel detector enables the dual-exposure DE technique to be integrated into the traditional workflow. Therefore, the aim of this study was to evaluate the effectiveness of the dual-exposure DE technique in flat-panel chest radiography for pulmonary nodule detection.

Materials and Methods

Patients

From August to October 2004, 100 consecutive patients (57 men and 43 women; mean age, 60.2 years; range, 18-89 years) from different clinical departments underwent chest CT and dual-exposure DE chest radiography in our hospital. Chest CT was performed within one month before or after the time of chest radiography. Fifty-two of the 100 patients had one or more pulmonary nodules. The median size of the pulmonary nodules was 1.0 cm (range 0.4-5 cm). The other 48 patients had no pulmonary nodules.

Chest radiography

Chest radiographs were acquired using a flat-panel digital chest system (Revolution XR/d, GE Medical Systems, Milwaukee, WI). The chest system includes a CsI scintillator and an amorphous silicon photodiode-transistor array. The detector has an image size of 41×41 cm and pixel dimension of 0.2×0.2 mm.

The DE examination consisted of the standard digital PA radiograph as well as the soft-tissue image and the bone image. DE images were acquired in a dual-exposure technique with 200 msec between the high- and low-energy exposures. The imaging parameters included a 140-kV image at a speed equivalent of approximately 250, and a 60-kV image at a speed equivalent of approximately 1,000 (Figs. 1A-C).

CT

CT examinations were performed using a multidetector CT (LightSpeed Ultra 16, GE Medical Systems) at 120 kV, 180 mA; collimation, 20 mm; table speed, 35 mm/rotation; scan time, 0.6 sec/rotation; reconstruction interval, 10 mm, or a single helical CT (Xvigor, Toshiba Medical Systems, Tokyo, Japan) at 120 kV, 160 mA; collimation, 10 mm; table speed, 12 mm/rotation; scan time, 1 sec/rotation; reconstruction interval, 10 mm (Figs. 1D, E).

Display

All digital images were sent to a picture archiving and communication systems (PACS) workstation (SYNAPSE, FujiFilm Medical Co., Ltd., Tokyo, Japan). All digital images were viewed on a 21-inch (53 cm) monochrome liquid crystal display (LCD) monitor (FC2090, Eizo Nanao Corp., Ishikawa, Japan) with a resolution of 1,536×2,048.

Quality of subtraction images

Before the reading test, the quality of subtraction images was evaluated on the basis of consensus of two experienced chest radiologists (M.U. and Y.Y.). Subtraction images were evaluated as fitting one of the following four grading descriptions: "excellent": few mismatch artifacts of pulmonary structures; "good": some mismatch artifacts of pulmonary structures, but the image is still suitable for diagnosis; "acceptable": in spite of the presence of some severe mismatch artifacts of pulmonary structures, an excess of 50% of the lung fields is suitable for diagnosis; and "not acceptable": there is poor matching of the whole lung, and the results are not acceptable for diagnosis.

Image evaluation

Ten radiologists participated in this study as observers: 5 residents with 4 or fewer years of experience and 5 experienced radiologists with 6 or more years of experience. CT examination served as the gold standard to determine the exact size and location of pulmonary nodules. Two other experienced chest radiologists (M.U. and Y.Y.) reviewed the CT images with consensus. Observers were not given any clinical information, including diagnoses and results of CT examination, except for patients' age and sex. The chest radiographs were presented as standard PA images alone or as standard PA radiographs in conjunction with DE subtraction images. Standard and DE sets were viewed in two sessions separated by one week. Images were presented in random order. No limit was imposed on reading time. The reading time was recorded in each session. A continuous rating scale of 0-100 was used to represent each observer's confidence level regarding the presence or absence of pulmonary nodules. The lungs were divided into two fields (right and left) for observation of pulmonary nodules.

Data and statistical analysis

Data are expressed as means ± standard deviation (SD). A total of 4,000 observations (100 patients × 2 fields × 2 sessions × 10 observers) were evaluated. Observer performance for the detection of pulmonary nodules with and without subtraction images was tested by using receiver operating characteristic (ROC) analysis of individual and averaged reader data.[10] Detection accuracy was measured according to the area under the ROC curve (Az), or Az value determined by ROCKIT (Metz CE, Department of Radiology, University of

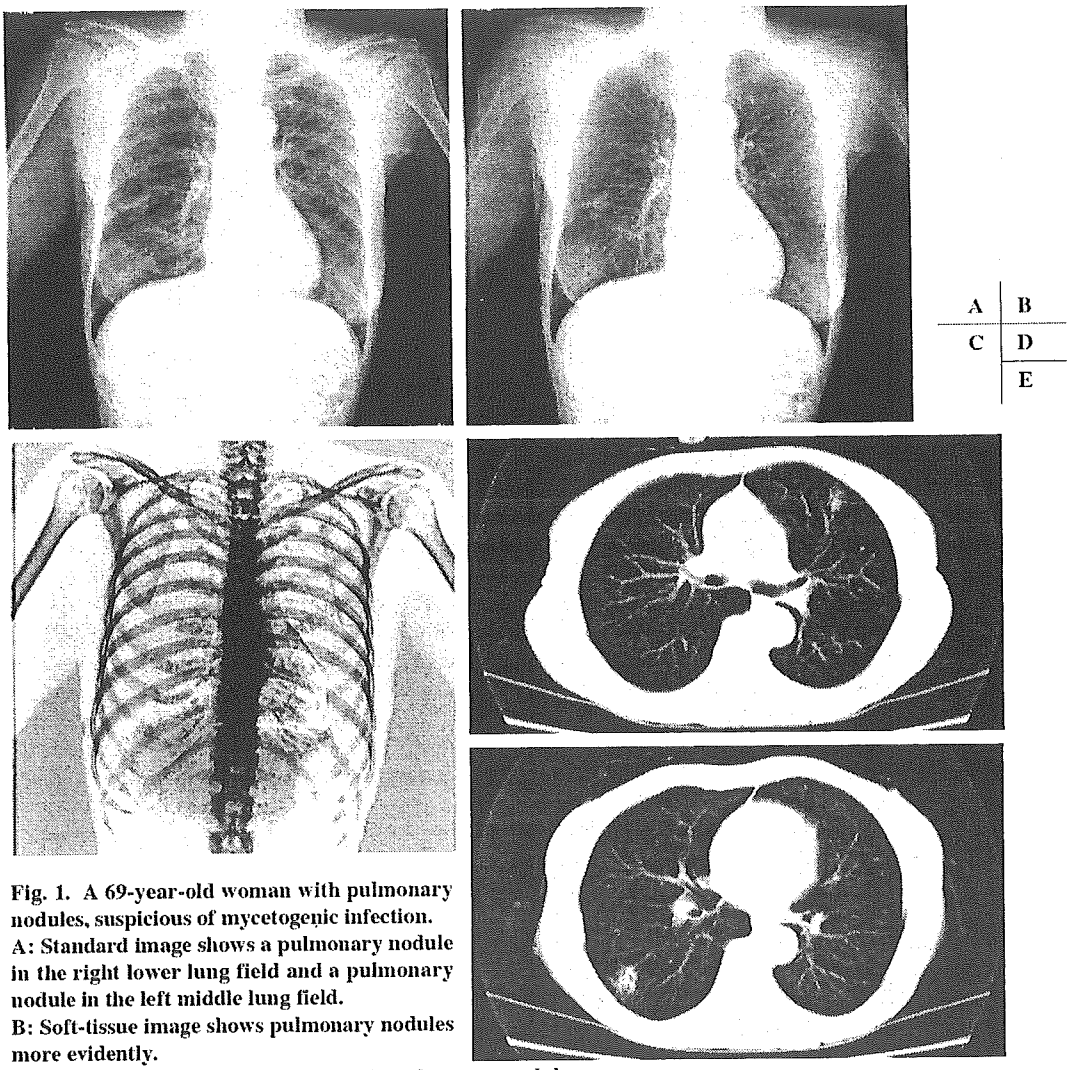

Fig. 1. A 69-year-old woman with pulmonary nodules, suspicious of mycetogenic infection.
A: Standard image shows a pulmonary nodule in the right lower lung field and a pulmonary nodule in the left middle lung field.
B: Soft-tissue image shows pulmonary nodules more evidently.
C: Bone image shows no calcification in pulmonary nodules.
D: CT image shows pulmonary nodule 1.5 cm in diameter in the upper lobe of the left lung.
E: CT image shows pulmonary nodule 2.1 cm in diameter in the lower lobe of the right lung.

Chicago, IL). The statistical significance of difference between the Az value with and without subtraction images and that between the reading time with and without them were determined with Student's two-tailed t-test for paired data. In addition, the statistical significance of the difference between the Az value for residents and that for experienced radiologists was determined with Student's two-tailed t-test. Probability values <0.05 were considered statistically significant.

Results

Results of visual evaluation of the quality of subtraction images are summarized in Table 1. Ninety-eight percent of the images of the right lung and 94% of the images of the left lung were evaluated to be excellent or good. Almost all images were assessed as acceptable for the reading test in both lung fields.

The observer study results are shown in Table 2. All ROC curves are illustrated in Figs. 2-5. The average Az value for the 10 observers increased significantly from 0.784 ± 0.029 without subtraction images to 0.815 ± 0.021 with subtraction images. The average Az value for residents increased significantly from 0.762 ± 0.016 without subtraction images to 0.803 ± 0.015 with subtraction images. Similarly the average Az value for experienced radiologists increased significantly from 0.805 ± 0.023 without subtraction

Table 1. Evaluation of the quality of subtraction images

Grade	Right lung	Left lung
	Number (%)	Number (%)
Excellent	88 (88)	68 (68)
Good	10 (10)	26 (26)
Acceptable	1 (1)	5 (5)
Not acceptable	1 (1)	1 (1)

Table 2. Az values of ROC curves for detection accuracy

Observer number	Az value	
	Without subtraction images	With subtraction images
Residents		
1	0.753	0.796
2	0.790	0.822
3	0.764	0.811
4	0.751	0.805
5	0.755	0.783
Mean Az value	0.762±0.016	0.803±0.015
Radiologists		
1	0.778	0.797
2	0.808	0.841
3	0.790	0.821
4	0.812	0.821
5	0.838	0.854
Mean Az value	0.805±0.023	0.827±0.022
All observers		
Mean Az value	0.784±0.029	0.815±0.021

images to 0.827±0.022 with subtraction images. In the comparison between residents and experienced radiologists, the average Az value for the experienced radiologists was significantly higher than that for the residents in the reading test without subtraction images (p=0.010). However, there was no significant difference between the Az value for residents and radiologists with subtraction images (p=0.083).

Meanwhile, for both subgroups of residents and experienced radiologists, there was no significant difference between the mean reading time per session without and with subtraction images (74.2 min vs. 75.0 min, p=0.796 for residents, 63.2 min vs. 68.2 min, p=0.261 for experienced radiologists). There was no significant difference between the mean reading time per session without and with subtraction images (Table 3, p=0.251).

Discussion

In the present study, we showed significant improvement in pulmonary-nodule detection by the addition of DE images for the first time with a flat-panel detector system. Significant improvement in nodule detection was obtained by the addition of DE images in all observers and in the subgroups of residents and experienced radiologists. Above all, the improvement of detectability of nodules was more pronounced in residents. With additional DE subtraction images, the nodule detectability of residents was improved to nearly the same level as that of experienced radiologists. This means that the DE technique would compensate for experience-dependent differences in diagnostic accuracy in the detection of pulmonary nodules. Considering that chest radiography is usually the first screening method for chest diseases and that the reader of chest radiographs is not usually an experienced chest radiologist, we conclude that the subtraction technique would be useful for reducing missed detection of pulmonary nodules in routine clinical practice.

Full-field digital amorphous silicon flat-panel x-ray

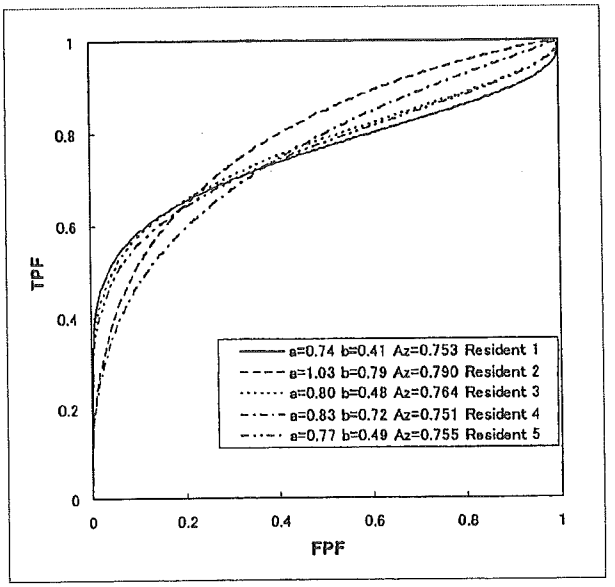

Fig. 2. Without subtraction images, ROC curve shows the detection accuracy of individual residents.
TPF: true-positive fraction, FPF: false-positive fraction.

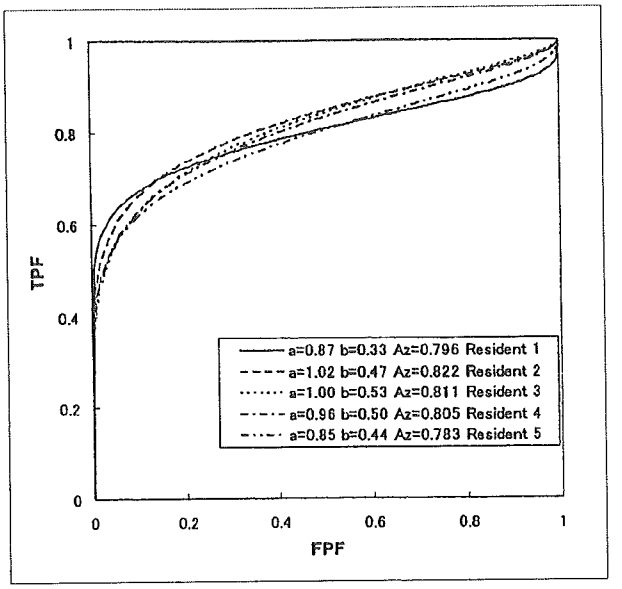

Fig. 3. With subtraction images, ROC curve shows the detection accuracy of individual residents.
TPF: true-positive fraction, FPF: false-positive fraction.

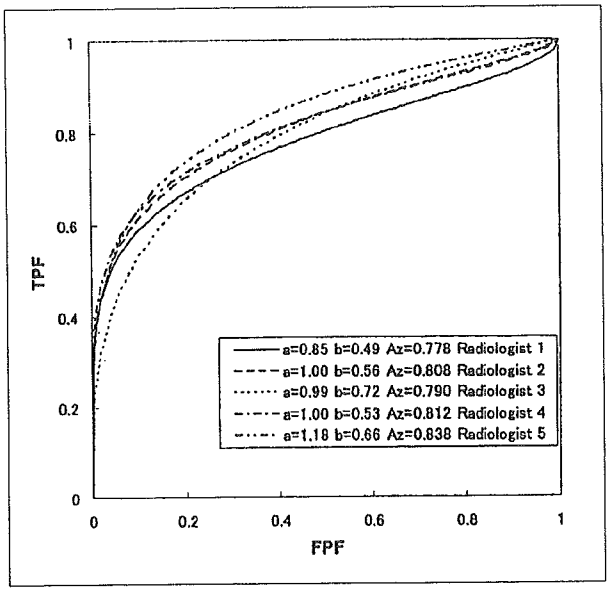

Fig. 4. Without subtraction images, ROC curve shows the detection accuracy of individual radiologists.
TPF: true-positive fraction, FPF: false-positive fraction.

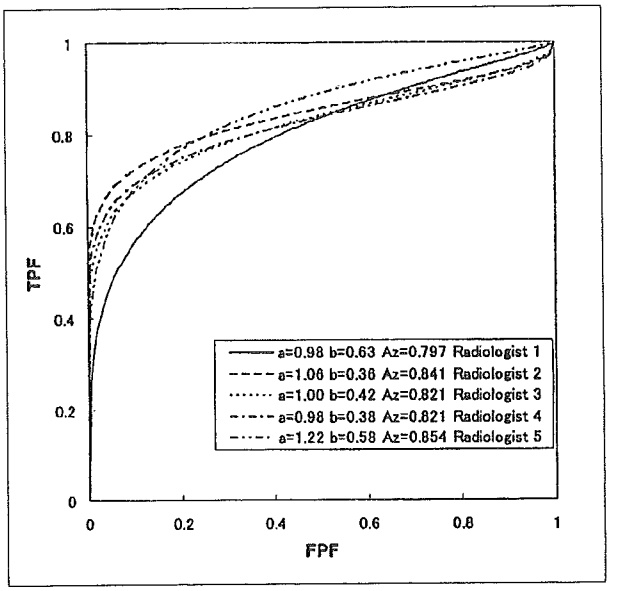

Fig. 5. With subtraction images, ROC curve shows the detection accuracy of individual radiologists.
TPF: true-positive fraction, FPF: false-positive fraction.

detector radiography systems based on CsI and amorphous silicon have recently become commercially available. Previous experimental and clinical studies have shown that excellent image quality is achieved with the silicon flat-panel x-ray detector radiography system compared with the image quality produced by conventional film-screen radiography and computed radiography systems.[11-13] Recent development of a fast, high-efficiency flat-panel detector enables the dual-exposure DE technique to be integrated into the traditional workflow. In this study, DE chest radiographs were acquired using a flat-panel digital chest system with

Table 3. Reading time of each observation

Observer number	Reading time (minutes)	
	Without subtraction images	With subtraction images
Residents		
1	99	92
2	80	80
3	54	54
4	81	81
5	57	68
Mean reading time	74.2±18.7	75.0±14.5
Radiologists		
1	90	86
2	39	55
3	58	68
4	61	58
5	68	74
Mean reading time	63.2±18.4	68.2±12.5
All observers		
Mean reading time	68.7±18.4	71.6±13.3

the dual-exposure technique. To our knowledge, there have been no conclusive studies using this system with the DE technique, and having a relatively large number of patients.

An important characteristic of the flat-panel detector radiography system is that its detective quantum efficiency (DQE) is higher than those of computed radiography and film-screen radiography systems.[12,14] A higher DQE provides improved capability to reveal an object in a noisy background,[14] in addition to the possibility of reducing patient radiation dose with no loss of diagnostic information. In previous studies, the flat-panel detector radiography system showed marked and significant dose reduction compared with that possible with computed radiography or film-screen radiography systems.[13,15,16] The flat-panel detector radiography system had equal image quality with approximately half the radiation dose, compared with computed radiography systems or film-screen radiography systems. Therefore, the dual-exposure technique with flat-panel detector does not increase radiation dose compared with these systems.

The quality of subtraction images was good. In the comparison between the right and left lung, mismatch artifacts were seen more frequently in the left lung. These were seen mostly in the left middle and lower fields. We considered that this would be influenced by heart beat. Although misregistration is one of the disadvantages of the dual-exposure technique, subtraction images of almost all cases were acceptable for reading.

Reading with subtraction images including soft-tissue and bone images did not require extended reading time compared with that without subtraction images. This would be caused by an increase in the confidence level of pulmonary nodule detection. Moreover, evaluation by the LCD monitor may take effect. Even without hard-copy films, observers could read images efficiently.

There are several limitations to our study. First, patients with relatively large masses or multiple nodules were included in the study. They could be easily detected without subtraction images. Subtraction images would be more beneficial for the detection of subtle lesions. In this regard, we may have underestimated the effectiveness of using the DE subtraction technique. Second, we evaluated only the detectability of pulmonary nodules, and did not evaluate qualitative diagnosis. The improvement in differential diagnosis between benign and malignant nodules with use of this method was not evaluated. Further studies should address the effect of this technique on the efficacy of pulmonary lesion classification.

In conclusion, dual-exposure DE subtraction chest radiography significantly improves the detection of pulmonary nodules without extending the reading time. The results indicate that the use of DE subtraction images is beneficial both for subgroups of residents and for experienced radiologists. Thus, this technique would be useful for reducing missed detection of pulmonary nodules in routine clinical practice.

Acknowledgments

We thank Dr. Seishi Kumano, Dr. Masaaki Hirata, Dr. Takatoshi Senba, Dr. Teruhito Kido, Dr. Noriko Hirose, Dr. Yuma Inoue, and Kohei Hosokawa, for participating as observers. We thank Mr. Yoshio Moribe, GE Yokogawa Medical Systems, for technical advice.

References

1) Kundel HL. Predictive value and threshold detectability of lung tumors. *Radiology*, 139: 25–29, 1981.
2) Kelcz F, Zink FE, Peppler WW, Kruger DG, Ergun DL, Mistretta CA. Conventional chest radiography vs. dual-energy computed radiography in the detection and characterization of pulmonary nodules. *AJR Am J Roentgenol*, 162: 271–278, 1994.
3) Brody WR, Butt G, Hall A, Macovski A. A method for selective tissue and bone visualization using dual energy scanned projection radiography. *Med Phys*, 8: 353–357, 1981.
4) Avinash GB, Jabri KN, Uppaluri R, *et al*. Effective dose reduction in dual-energy flat panel X-ray imaging: technique and clinical evaluation. *Proceedings of SPIE*, 4684: 1048–1059, 2002.
5) Niklason LT, Hickey NM, Chakraborty DP, *et al*. Simulated pulmonary nodules: detection with dual-energy digital versus conventional radiography. *Radiology*, 160: 589–593, 1986.
6) Ishigaki T, Sakuma S, Ikeda M. One-shot dual-energy subtraction chest imaging with computed radiography: clinical evaluation of film images. *Radiology*, 168: 67–72, 1988.
7) Oestmann JW, Greene R, Rhea JT, *et al*. "Single-exposure" dual energy digital radiography in the detection of pulmonary nodules and calcifications. *Invest Radiol*, 24: 517–521, 1989.
8) Kido S, Ikezoe J, Naito H, *et al*. Clinical evaluation of pulmonary nodules with single-exposure dual-energy subtraction chest radiography with an iterative noise-reduction algorithm. *Radiology*, 194: 407–412, 1995.
9) Chotas HG, Dobbins JT 3rd, Ravin CE. Principles of digital radiography with large-area, electronically readable detectors: a review of the basics. *Radiology*, 210: 595–599, 1999.
10) Metz CE. ROC methodology in radiologic imaging. *Invest Radiol*, 21: 720–733, 1986.
11) Rong XJ, Shaw CC, Liu X, Lemacks MR, Thompson SK. Comparison of an amorphous silicon/cesium iodide flat-panel digital chest radiography system with screen/film and computed radiography systems—a contrast-detail phantom study. *Med Phys*, 28: 2328–2335, 2000.
12) Garmer M, Hennigs SP, Jager HJ, *et al*. Digital radiography versus conventional radiography in chest imaging: diagnostic performance of a large-area silicon flat-panel detector in a clinical CT-controlled study. *AJR Am J Roentgenol*, 174: 75–80, 2000.
13) Fink C, Hallscheidt PJ, Noeldge G, *et al*. Clinical comparative study with a large-area amorphous silicon flat-panel detector: image quality and visibility of anatomic structures on chest radiography. *AJR Am J Roentgenol*, 178: 481–486, 2002.
14) Floyd CE, Warp RJ, Dobbins JT 3rd, *et al*. Imaging characteristics of an amorphous silicon flat-panel detector for digital chest radiography. *Radiology*, 218: 683–688, 2001.
15) Strotzer M, Gmeinwieser JK, Volk M, Frund R, Seitz J, Feuerbach S. Detection of simulated chest lesions with normal and reduced radiation dose: comparison of conventional screen-film radiography and a flat-panel X-ray detector based on amorphous silicon. *Invest Radiol*, 33: 98–103, 1998.
16) Bacher K, Smeets P, Bonnarens K, De Hauwere A, Verstraete K, Thierens H. Dose reduction in patients undergoing chest imaging: digital amorphous silicon flat-panel detector radiography versus conventional film-screen radiography and phosphor-based computed radiography. *AJR Am J Roentgenol*, 181: 923–929, 2003.

Yasushi Koyama, MD
Hiroshi Matsuoka, MD
Teruhito Mochizuki, MD
Hiroshi Higashino, MD
Hideo Kawakami, MD
Shigeru Nakata, RT
Jun Aono, MD
Taketoshi Ito, MD
Makiko Naka, MS
Yasuo Ohashi, PhD
Jitsuo Higaki, MD

Published online before print
10.1148/radiol.2353030441
Radiology 2005; 235:804–811

Abbreviations:
CK = creatine kinase
ECG = electrocardiography
EDV = end-diastolic volume
EF = ejection fraction
ESV = end-systolic volume
MI = myocardial infarction
TIMI = Thrombolysis in Myocardial Infarction

[1] From the Departments of Cardiology (Y.K., H.M., H.K., J.A., T.I.) and Radiology (H.H.), Ehime Prefectural Imabari Hospital, 4-5-5 Ishii-chou, Imabari, 794-0006, Ehime, Japan; Department of Radiology (T.M., S.N.) and Second Department of Internal Medicine (J.H.), Ehime University School of Medicine, Ehime, Japan; and Department of Biostatistics/Epidemiology and Preventive Health Sciences, School of Health Sciences and Nursing, University of Tokyo, Tokyo, Japan (M.N., Y.O.).
From the 2002 RSNA Annual Meeting. Received March 22, 2003; revision requested June 13; final revision received July 27, 2004; accepted August 16. Address correspondence to Y.K. (e-mail: *yasushi@koyamasan.com*).

Authors stated no financial relationship to disclose.

Author contributions:
Guarantors of integrity of entire study, Y.K., T.M., T.I., J.H.; study concepts and design, Y.K., T.M., T.I., J.H.; literature research, Y.K., H.M., T.M., H.H., H.K., T.I., J.H.; clinical studies, Y.K., H.M., T.M., H.H., H.K., S.N., J.A., T.I., J.H.; experimental studies, Y.K., T.M., S.N., J.A., T.I., J.H.; data acquisition, Y.K., H.M., T.M., H.H., H.K., J.A.; data analysis/interpretation, Y.K., T.M., H.H., H.K., T.I., J.H.; statistical analysis, Y.O., M.N., Y.K.; manuscript preparation, Y.K.; manuscript definition of intellectual content, Y.K., T.M.; manuscript editing and final version approval, all authors; manuscript revision/review, Y.K., T.M., T.I., M.N., Y.O., J.H.

Assessment of Reperfused Acute Myocardial Infarction with Two-Phase Contrast-enhanced Helical CT: Prediction of Left Ventricular Function and Wall Thickness[1]

PURPOSE: To investigate whether two-phase contrast material–enhanced computed tomographic (CT) findings serve as predictors of changes in left ventricular (LV) function and wall thickness (WT) after acute myocardial infarction (MI) and successful angioplasty.

MATERIALS AND METHODS: Ethics committee approval and informed consent were obtained. In 58 patients (51 men and seven women; mean age, 62 years ± 12 [standard deviation]) who had experienced an acute MI and undergone successful angioplasty, two-phase (acquisitions at 45 seconds and 7 minutes) contrast-enhanced CT was performed in the acute (mean interval between treatment and CT, 37 hours ± 4) and intermediate (mean interval, 28 days ± 4) periods and for long-term (mean interval, 12 months ± 4) follow-up. CT images were reviewed for an early perfusion defect (ED) at 45 seconds and for late enhancement (LE) and a residual perfusion defect (RD) at 7 minutes. Myocardial enhancement patterns and WT were assessed, and LV ejection fraction (LVEF) and percentage decrease in WT were calculated. The patient group was subdivided into three groups according to enhancement pattern: Group 1 included patients with LE but no ED or RD; group 2, patients with ED and LE but no RD; and group 3, patients with ED, LE, and RD. Fisher exact testing was used to measure categorical response. Paired and unpaired *t* tests were used for comparison between two groups (points); Tukey-Kramer multiple comparison and repeated-measures analysis of variance were used for comparisons between the three groups. $P < .05$ was considered to indicate a significant difference.

RESULTS: In group 3 ($n = 36$), WT in infarcted area was significantly reduced at the intermediate and long-term CT examinations ($P < .001$). At the intermediate and long-term examinations, percentage decrease in WT was greater in group 2 ($n = 10$) than in group 1 ($n = 12$) ($P < .05$ for intermediate and $P < .001$ for long-term examination) and was greatest in group 3 ($P < .001$ for both examinations). LVEF was poorest in group 3 and best in group 1.

CONCLUSION: Two-phase contrast-enhanced CT proved useful in predicting LV functional recovery and WT in patients who had experienced acute MI and undergone successful angioplasty.
© RSNA, 2005

Previous researchers (1,2) have proposed the use of a reconstruction algorithm with an electrocardiographically (ECG)-gated or non–ECG-gated technique at single-section helical computed tomography (CT) (3) for cardiac imaging. Multi–detector row CT has been developed in recent years as the temporal resolution of helical CT has improved, and CT has thus become a useful tool for coronary artery imaging (4–6).

Because the prognosis of patients who have experienced an acute myocardial infarction (MI) depends on their myocardial reperfusion status, the assessment of microvascular flow after reperfusion therapy is of great importance.

Conventionally, myocardial perfusion is evaluated mainly by using nuclear imaging techniques (7,8). Contrast material–enhanced magnetic resonance (MR) imaging (9–12) and myocardial contrast echocardiography (13–15) are also common procedures that can be employed to assess myocardial perfusion. Electron-beam CT also provides reliable information on myocardial perfusion (16). In a case report, contrast-enhanced helical CT revealed an early myocardial perfusion defect and late enhancement in acute MI, and these findings agree with those observed at nuclear imaging and contrast-enhanced MR imaging (17), suggesting a possible use for contrast-enhanced helical CT in myocardial perfusion assessment.

The goal of this study was to investigate whether two-phase contrast-enhanced CT findings serve as predictors of changes in left ventricular function and wall thickness in patients who have experienced acute MI and have undergone successful reperfusion therapy.

MATERIALS AND METHODS

Initial Study Population

Our study initially included 65 consecutive patients enrolled between October 1999 and March 2001: 59 patients who had experienced acute MI and had undergone successful reperfusion therapy and six patients who had experienced acute MI, had undergone successful reperfusion therapy, and had previously undergone part of the study protocol that was later used with the other 59 patients. These six patients agreed to complete the protocol used with the other 59 patients. The study protocol was approved by the ethics committee of Ehime Prefectural Imabari Hospital, and all patients gave their informed consent.

Inclusion Criteria

Inclusion criteria consisted of the following:

1. The presence of typical symptoms of acute MI associated with ECG changes and a serum concentration of creatine kinase (CK) of more than twice the upper limit of normal with more than 5% of the isoenzyme CK-MB in the serum.

2. A first acute MI that was related to a single coronary artery.

3. Successful coronary angioplasty of the totally or subtotally occluded infarct-related artery (Thrombolysis in Myocardial Infarction [TIMI] grade 0 or 1) within 12 hours after the onset of chest pain. In brief, TIMI grade 0 perfusion indicates that there is no antegrade flow beyond the point of occlusion, grade 1 indicates minimal incomplete perfusion of a contrast medium around the clot, grade 2 (partial perfusion) indicates complete but delayed perfusion of the distal coronary bed with a contrast medium, and grade 3 (complete perfusion) indicates antegrade flow to the entire distal coronary bed at a normal rate.

4. Residual stenosis of less than 50% after angioplasty.

Exclusion Criteria

Exclusion criteria consisted of the following:

1. Renal failure (serum creatinine level > 1.5 mg/dL [132.6 μmol/L] and/or blood urea nitrogen level > 21 mg/dL [7.5 μmol/L]).

2. Restenosis of 50% or greater at coronary angiography during follow-up.

3. Inadequate CT imaging and/or cine angiographic results.

4. Lipid degeneration or calcification in the myocardium on non–ECG-gated 10-mm-thick plane scans obtained before the contrast-enhanced CT examination was performed.

Seven patients were excluded from the analysis because of the following reasons: Their cineangiograms were inadequate for evaluation of TIMI flow grade ($n = 2$), they had incomplete coronary recanalization (residual stenosis ≥ 50% owing to distal embolization) ($n = 1$), restenosis was detected at coronary angiography during follow-up ($n = 2$), or their CT images were inadequate because of atrial fibrillation ($n = 1$) or body movement ($n = 1$).

Final Study Population

Therefore, this study is based on data from 58 evaluable patients (mean age, 62 years ± 12 [standard deviation]; age range, 39–84 years): 51 men (mean age, 62 years ± 11; age range, 39–83 years) and seven women (mean age, 66 years ± 14; age range, 46–84 years). According to results of unpaired t testing, there were no significant differences between the male and the female patients in terms of age. The left anterior descending artery was involved in 31 patients, the right coronary artery was involved in 23 patients, and the circumflex artery was involved in four patients. Fifty-seven patients (98%) underwent stent placement, and one patient (2%) underwent balloon angioplasty. Regarding the final TIMI grade, 56 patients (97%) had TIMI grade 3 reflow, and two patients (3%) had TIMI grade 2 reflow.

Study Protocol

Coronary angiography was performed in all 58 patients who underwent angioplasty. In the acute phase study, conventional left ventriculography was performed immediately after coronary angioplasty, which was performed by one of three cardiologists (T.I., H.M., and J.H., with 25, 23, and 30 years of clinical practice, respectively), to assess end-diastolic volume (EDV), end-systolic volume (ESV), and ejection fraction (EF). Two-phase contrast-enhanced CT was performed within 48 hours (mean interval, 37 hours ± 4) after direct angioplasty. In the intermediate phase study, both coronary angiography and left ventriculography were performed a mean of 27 days ± 3 after direct angioplasty, and two-phase contrast-enhanced CT was performed a mean of 28 days ± 4 after direct angioplasty. In the long-term study, two-phase contrast-enhanced CT was performed 12 months ± 4 after direct angioplasty. The biplanar angiographic system used for coronary angiography and conventional left ventriculography was an Integris V3000 (Philips Medical Systems, Best, the Netherlands). A Cardio 500 analysis system (Kontron Electronik, Munich, Germany) was used for performing quantitative coronary angiography and assessing cardiac function. During the infusion of the contrast medium (Optiray [320 milligrams of iodine per milliliter]; Yamanouchi, Tokyo, Japan) at a rate of 8 mL/sec to a total of 35 mL, biplanar images were obtained at a filming rate of 30 images per second.

Two-Phase Contrast-enhanced CT

The helical CT scanner used was a single-detector row Proceed SA (GE-Yokogawa Medical Systems, Tokyo, Japan) with a gantry rotation speed of 0.8 second. Patients were asked to lie supine on the CT table and inhale oxygen at a rate of 3 L/min while the scanning parameters were prepared.

The scanning protocol was based on that used in a previous study involving electron-beam CT (16) and was as fol-

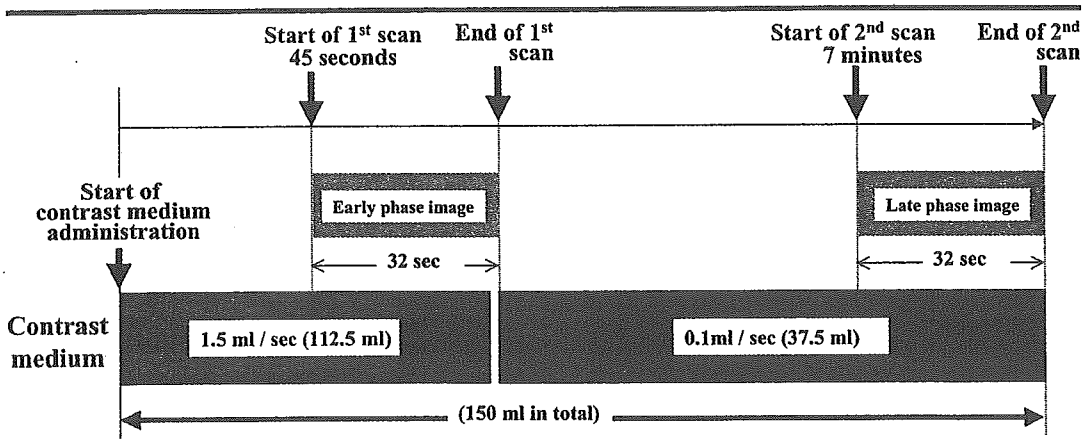

Figure 1. Protocol for two-phase contrast-enhanced CT.

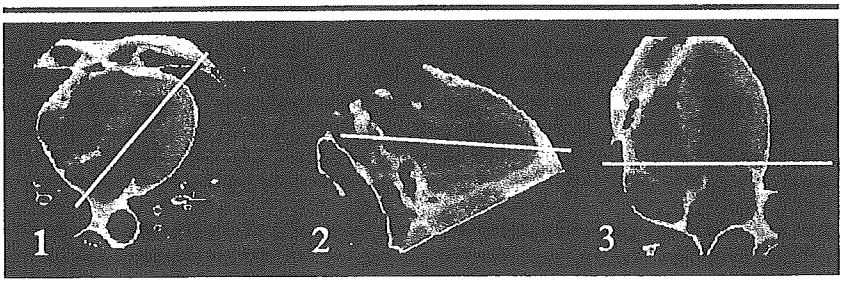

Figure 2. Schematic representation of double-oblique method for acquiring short-axis images. The CT images are reversals in white and black. *1,* Transaxial image obtained at end diastole shows the first oblique plane (line) in the long axis of the transaxial image; from this we obtained the long-axis view in *2. 2,* The second image was then obliqued at the line connecting the apex and the posterior base of the aortic valve (line); from this we obtained the four-chamber image in *3. 3,* On the four-chamber image, we "cut" the heart from its base (line) to the apex to obtain two-dimensional short-axis images.

lows: Nonionic iodinated contrast medium (iopamidol, Iopamiron [300 milligrams of iodine per milliliter]; Nihon Schering, Osaka, Japan) was intravenously administered at a rate of 1.5 mL/sec for the first acquisition for the early image. The early image was obtained 45 seconds after the start of contrast medium administration; the same contrast medium was then infused at a rate of 0.1 mL/sec for the second acquisition for the late image. The late image was obtained 7 minutes after the start of contrast medium administration; a total of 150 mL of the contrast medium was used (Fig 1). The ECG trace was recorded during scanning so that we could determine triggers and identify the diastolic image data set. Patients were asked to hold their breath during whole-heart scanning. Scanning parameters were as follows: collimation, 3 mm; table feed, 3 mm per rotation; and number of rotations, 40 (at a rate of 12 cm every 32 seconds). The tube current and voltage were 200 mA and 140 kV, respectively.

A partial 180° reconstruction algorithm was used, and the temporal resolution of one transaxial image was 0.4 second. The field of view was 180 mm, and the matrix was 512 × 512. Transaxial images were generated by using overlap reconstruction at a pitch of 0.1, and 391 3-mm-thick transaxial images, at intervals of 0.3 mm (0.08 second), including various cardiac phases, were obtained (1). The weighted CT dose index, as defined in reference 18, was 9.4 mGy for one acquisition.

The diastolic image data set, which was extracted with reference to the R wave of the recorded ECG trace, was used to assess myocardial enhancement pattern and wall thickness. The 3-mm-thick cardiac short-axis images were reconstructed by using the double-oblique method (Fig 2). All measurements were performed by using a ZIO-M900 workstation (ZIO Software, Tokyo, Japan).

Assessment of Myocardial Enhancement with Two-Phase Contrast-enhanced CT

All patient-identifying information on the CT images was obscured; the images were then randomized. Two cardiologists (T.I. and Y.K., with 25 and 10 years of clinical practice, respectively) and two radiologists (H.H. and T.M., with 20 and 25 years of clinical practice, respectively), who were blinded to patient treatment information, visually judged the myocardial enhancement pattern together. Disagreements were solved by consensus.

We defined a myocardial perfusion defect (a dark zone) on the early-phase images (those obtained 45 seconds after contrast material administration) as an early perfusion defect, the presence of smaller dark regions in the subendocardium surrounded by partially enhanced myocardium on the late-phase images (those obtained 7 minutes after contrast material administration) as a residual perfusion defect, and the presence of an enhanced zone on the late-phase images as late enhancement.

Regions of interest were created for one-third of the area of each finding (early perfusion defect, residual defect, and late enhancement) and were placed over the center of each area. A region of interest of the same size, which was at least greater than 50 mm^2, was also placed over a remote noninfarcted area on the opposite side of the infarct-related area so that we could measure the mean attenuation. This was performed by the same four investigators (T.I., Y.K., H.H., and T.M.) working in consensus.

Enhancement Patterns

Several enhancement patterns theoretically exist; however, all enhancement could actually be classified into one of the following three patterns: group 1, in which there is an absence of early perfusion defect in the early phase and a presence of late enhancement without residual perfusion defect in the late phase; group 2, in which there is a presence of early perfusion defect in the early phase and a presence of late enhancement without residual perfusion defect in the late phase; and group 3, in which there is a presence of early perfusion defect in the early phase and a presence of both late enhancement and residual perfusion defect in the late phase (Fig 3).

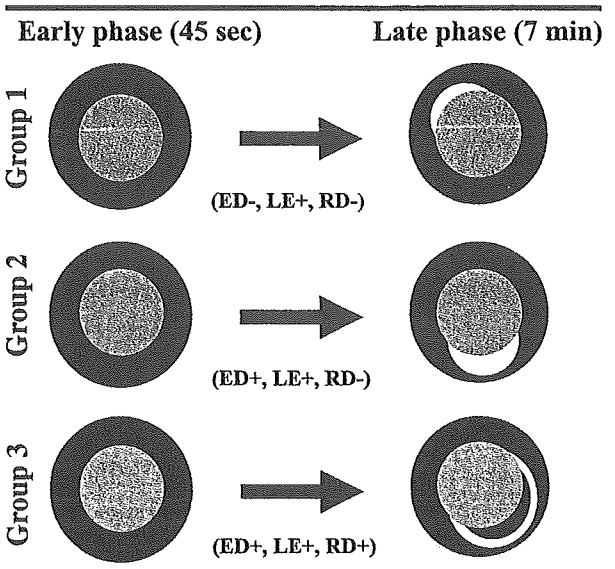

Figure 3. Schematic representation of the enhancement pattern observed on short-axis two-phase contrast-enhanced CT images in each group. The dark gray circles indicate the left ventricular wall; the light gray circles indicate the left ventricular cavity. Group 1 had no early perfusion defect *(ED;* black regions in left column*)* on the early image and had late enhancement *(LE;* white regions*)* without a residual perfusion defect *(RD;* black region in right column*)* on the late image, group 2 had an early perfusion defect and late enhancement without a residual perfusion defect, and group 3 had both an early and a residual perfusion defect with partial late enhancement.

Wall Thickness

Wall thickness was measured by the same four investigators (T.I., Y.K., H.H., and T.M.) in consensus by using an early-phase end-diastolic short-axis image. The measured points in the acute phase, intermediate phase, and long-term studies were the infarct-related and the noninfarcted areas. We calculated the percentage decrease in wall thickness, or WT_{pd}, in the intermediate phase and long-term studies as follows: $WT_{pd} = [(WT_a - WT_i \text{ or } WT_l)/WT_a] \cdot 100$, where WT_a is the wall thickness observed during the acute phase study, WT_i is that observed during the intermediate phase study, and WT_l is that observed during the long-term study.

In the long-term study, a scar was defined according to published criteria based on autopsy data (19). If the myocardial segment was thin on the early-phase images (wall thickness, <6 mm), the patient was given a diagnosis of transmural scar formation.

Analysis of Conventional Coronary Angiographic and Left Ventriculographic Results

All patient-identifying information on the coronary angiograms was obscured; the angiograms were then randomized. Two cardiologists (H.M. and H.K., with 23 and 14 years of clinical practice, respectively), who were blinded to patient clinical outcome, classified in simultaneous consensus the antegrade contrast material flow in the infarct-related artery on the final coronary angiograms according to the criteria established by the TIMI study group. All patient-identifying information on the conventional left ventriculograms was obscured; the ventriculograms were then randomized. Two observers (J.H. and J.A., with 30 and 14 years of clinical practice, respectively) measured EDV and ESV and calculated the left ventricular EF by using the area-length method (20) and working in consensus.

Determination of Peak CK Level and CK-MB Fraction

Immediately after reperfusion therapy, blood was collected every 4 hours, and J.A. determined the maximum values of serum CK and the isoenzyme CK-MB.

Determination of Ischemic Time

Ischemic time was measured by J.A. and was defined as the interval from the onset of the symptoms to the time at which the first balloon inflation was performed.

Statistical Analysis

All data are expressed as means ± standard deviations. The Fisher exact test was used for comparing the frequencies of sex and culprit artery among the groups (group 1, group 2, and group 3). The Tukey-Kramer multiple comparison test was used for comparing age among the groups. An unpaired *t* test was used for comparing mean CT values in regions of interest of noninfarcted area, and the Tukey-Kramer multiple comparison test was used for comparing CT values between three areas (the region of interest of the noninfarcted area, the region of interest of the late enhancement area, and the region of interest of the residual perfusion defect area). The Tukey-Kramer multiple comparison test was also used for comparing ages, CK levels, CK-MB fractions, and ischemic time between the groups.

A paired *t* test was used for two-point comparisons (between the acute and the intermediate phase study) of EDV, ESV, and EF in each group. The Tukey-Kramer multiple comparison test was also used for group comparisons of EDV, ESV, and EF at two points (the acute and intermediate phase studies).

Regarding the wall thickness of the noninfarcted area, repeated analysis of variance measurement of groups, time points (the acute phase, intermediate phase, and long-term studies), and their interaction terms was performed. As a covariance structure among the time

Characteristics of 58 Patients according to Group

Characteristic	Group 1	Group 2	Group 3
No. of patients	12 (21)	10 (17)	36 (62)
Sex*			
Male	10 (83)	7 (70)	34 (94)
Female	2 (17)	3 (30)	2 (6)
Age (y)†	66 ± 11	68 ± 11	59 ± 11
Culprit artery*			
Right coronary	5 (42)	5 (50)	13 (36)
Left anterior descending	5 (42)	3 (30)	23 (64)
Circumflex	2 (17)	2 (20)	0
Clinical treatment			
Stent placement	12 (100)	10 (100)	35 (97)
Balloon angioplasty	0	0	1 (3)
Final TIMI grade			
2	0	0	2 (6)
3	12 (100)	10 (100)	34 (94)

Note.—Unless otherwise stated, data are numbers of patients, with percentages in parentheses. Percentages may not add up to 100% owing to rounding.

* No significant differences ($P \geq .05$) between groups (Fisher exact test).

† Data are mean values ± standard deviations. There were no significant differences ($P \geq .05$) in age between the groups (Tukey-Kramer multiple comparison test).

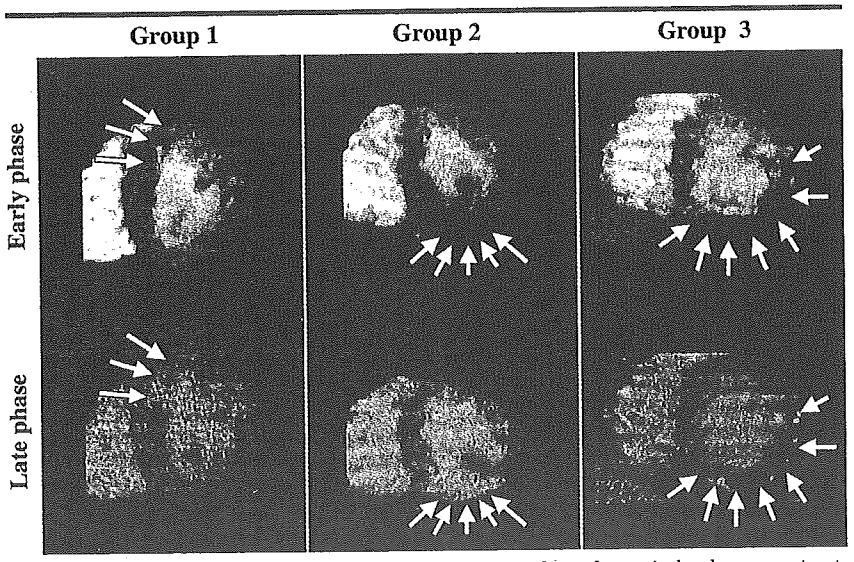

Figure 4. Short-axis contrast-enhanced helical CT images show the typical enhancement patterns in the three groups. Images obtained in 56-year-old man in group 1 with acute MI (arrows) in the territory of the left anterior descending coronary artery show no early perfusion defect and late enhancement without a residual defect. Images obtained in 62-year-old woman in group 2 with acute MI (arrows) in the territory of the right coronary artery show an early perfusion defect and late enhancement without a residual defect. Images obtained in 60-year-old man in group 3 with acute MI (arrows) in the territory of the circumflex coronary artery show an early defect and late enhancement with a residual defect.

points, compound symmetry was assumed and robust variance was used.

Regarding the wall thickness of the infarcted area, heterogeneity among individuals in the degree of damage due to infarction was expected, so we used the wall thickness at the acute phase study as an adjusting factor; repeated-measures analysis of variance with groups, time points (the intermediate phase and long-term studies), and their interaction terms was then performed. As a covariance structure among the time points, compound symmetry was assumed and robust variance was used.

The Tukey-Kramer multiple comparison test was used for group comparisons of percentage decrease in wall thickness at two points (the intermediate phase and long-term studies). A paired *t* test was used for two-point comparisons (between the intermediate phase and the long-term study) of percentage decrease in wall thickness in each group. $P < .05$ was considered to indicate a statistically significant difference. The statistical analyses were performed by using SAS version 8.2 (SAS Institute, Cary, NC).

RESULTS

Myocardial Enhancement Pattern at Two-Phase Contrast-enhanced CT

There were 12 patients in group 1, 10 patients in group 2, and 36 patients in group 3. Patient characteristics were not significantly different between the three groups (Table).

We found that the attenuation of early perfusion defects (30.2 HU ± 11) was significantly lower than that of the noninfarcted areas (102.1 HU ± 9.0, $P < .001$) on the early-phase (45-second) image. Areas with late enhancement (112.9 HU ± 18.5) had higher attenuation compared with areas with residual perfusion defect (59.3 HU ± 11, $P < .001$) and noninfarcted areas (88.6 HU ± 13.7, $P < .001$ vs areas with late enhancement, $P < .001$ vs areas with residual perfusion defect) on the late-phase (7-minute) images (Fig 4).

Peak CK Level, Peak CK-MB Fraction, and Ischemic Time

Peak CK (2555 U/L ± 1055) and CK-MB (194 U/L ± 89) values in group 2 were higher than those in group 1, which had a peak CK value of 904 U/L ± 270 ($P < .01$) and a peak CK-MB value of 87 U/L ± 43 ($P < .05$). Peak CK and CK-MB values, respectively, were highest in group 3 at 4111 U/L ± 1301 ($P < .001$) and 285 U/L ± 109 ($P < .05$). The ischemic time (the time elapsed from the first onset of symptoms to the first balloon inflation) was 282 minutes ± 93 in group 3 and was significantly longer than that in group 1 (170 minutes ± 59, $P < .001$). The ischemic time in group 2 (234 minutes ± 44) did not significantly differ from that in groups 1 and 3.

EDV, ESV, and EF in Acute and Intermediate Phase Studies: Intra- and Intergroup Comparisons

In group 1, between the time of the acute phase and the time of the intermediate phase study, the EDV did not change significantly (value at acute phase study, 129 mL ± 24; value at intermediate phase study, 121 mL ± 29 [$P = .069$]), the ESV decreased (value at acute phase

study, 51 mL ± 11; value at intermediate phase study, 28 mL ± 8 [$P < .001$]), and the EF improved (value at acute phase study, 60% ± 11; value at intermediate phase study, 76% ± 8 [$P < .001$]). In group 2, EDV, ESV, and EF did not change significantly: EDV decreased from 122 mL ± 24 to 115 mL ± 26, ESV decreased from 46 mL ± 12 to 43 mL ± 14, and EF increased from 62% ± 7 to 63% ± 8. In group 3, EDV increased from 121 mL ± 35 to 148 mL ± 37 ($P < .001$), ESV increased from 44 mL ± 21 to 72 mL ± 30 ($P < .001$), and EF decreased from 64% ± 11 to 52% ± 13 ($P < .001$). In the acute phase study, no significant differences were noted in EDV, ESV, or EF among the three groups.

In the intermediate phase study, the EDV in group 3 was the largest among the three groups ($P < .05$), the ESVs in groups 1 and 2 were smaller than the ESV in group 3 ($P < .001$ and $P < .01$, respectively), and the EF in group 1 was higher than that in group 3 ($P < .001$) and group 2 ($P < .05$). The EF in group 2 was higher than that in group 3 ($P < .05$).

Wall Thickness and Percentage Decrease in Wall Thickness

The wall thickness values in the noninfarcted area at three time points—the acute phase, intermediate phase, and long-term studies, respectively—were 12.0 mm ± 1.7, 12.2 mm ± 1.7, and 11.8 mm ± 1.7 in group 1; 11.0 mm ± 1.7, 11.1 mm ± 1.6, and 11.0 mm ± 1.7 in group 2; and 11.5 mm ± 2.1, 11.5 mm ± 2.0, and 11.2 mm ± 1.8 in group 3. There were no significant differences between the time points ($P = .058$), the groups ($P = .330$), or their interactions ($P = .181$) according to results of repeated-measures analysis of variance.

The wall thickness values in the infarcted area at three time points—the acute phase, intermediate phase, and long-term studies, respectively—were 11.7 mm ± 1.3, 11.6 mm ± 1.3, and 11.6 mm ± 1.5 in group 1; 11.1 mm ± 2.1, 9.1 mm ± 1.7, and 8.1 mm ± 1.7 in group 2; and 11.1 mm ± 1.9, 6.1 mm ± 1.7, and 4.8 mm ± 1.5 in group 3. There were no significant differences ($P = .657$) in wall thickness at the acute phase study among the groups. However, according to results of repeated-measures analysis of variance, there were significant differences within each group ($P < .001$) and among time points ($P = .001$), their interactions ($P < .001$), and adjusting factors ($P = .001$).

In group 3, 21 patients (58%) with transmural early perfusion defect were found to have scar formation. Figure 5 shows typical images obtained at the long-term study (in the same patients as in Fig 4) in these three groups.

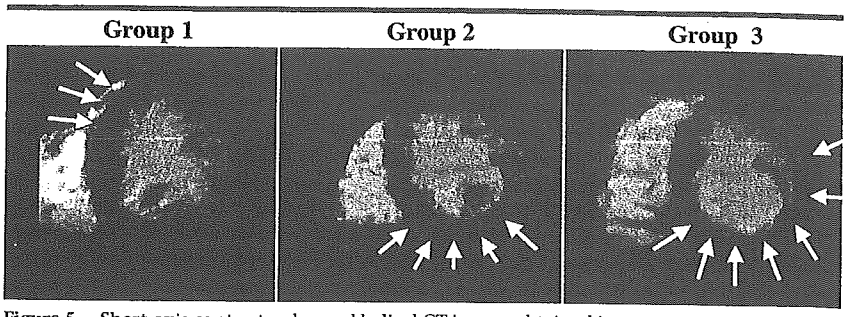

Figure 5. Short-axis contrast-enhanced helical CT images obtained in same patients as in Figure 4 show typical early phase findings in the three groups at the long-term study. In group 1, wall thickness in the infarcted area (arrows) did not change between the acute phase (as seen in upper left image of Figure 4) and the long-term studies. In group 2, wall thickness in the infarcted area (arrows) at the long-term study was moderately decreased compared with the thickness at the acute phase study (as seen in upper middle image of Figure 4). In group 3, wall thickness in the infarcted area (arrows) at the long-term study was significantly decreased compared with the thickness at the acute phase study (as seen in upper right image of Figure 4). In group 3, areas of transmural early defect with residual defect in the acute phase (as seen in group 3 images of Fig 4) changed to areas of scar formation at the long-term study.

As regards the infarcted area, because groups, time points (intermediate phase and long-term studies), and their interaction terms differed significantly, we tried to investigate the percentage decrease in wall thickness, which was based on the wall thickness at the acute phase study, at two points (the intermediate phase and long-term studies).

In terms of percentage decrease in wall thickness of the infarcted areas, there were no significant differences between group 1 and group 2 at the intermediate phase and long-term studies. The percentage decrease in wall thickness in group 3 at the long-term study was greater than that at the intermediate phase study ($P < .001$).

At the intermediate phase study, the percentage decrease in wall thickness of the infarcted areas in group 1 (0.4% ± 1.7) was the lowest among the three groups (group 2: 17.6% ± 9.8, $P < .05$; group 3: 44.4% ± 15.9, $P < .001$). The percentage decrease in wall thickness in group 3 was greater than that in group 2 ($P < .001$).

At the long-term study, the percentage decrease in wall thickness in group 3 (56.1% ± 4.2) was the highest among the three groups (group 1: 0.9% ± 3.6, $P < .001$; group 2: 26.5% ± 10.7, $P < .001$). The percentage decrease in wall thickness in group 2 was greater than that in group 1 ($P < .001$).

DISCUSSION

Our results show that, in patients with acute MI, the myocardial enhancement pattern at two-phase contrast-enhanced CT performed after reperfusion therapy could serve as a predictor of left ventricular functional recovery and wall thickness. Previous researchers have reported that mortality is reduced in patients with TIMI grade 3 flow (21–26). Gibson et al (27) reported that patients with both normal epicardial (TIMI grade 3) flow and normal tissue-level perfusion (TIMI myocardial perfusion grade 3) have an extremely low mortality risk.

Although revascularization of the epicardial coronary arteries (improvement of TIMI grade flow) is necessary for the myocardium to be salvaged, this is not enough to ensure myocardial recovery. That is, successful revascularization of epicardial coronary arteries is not equal to successful reperfusion at the microvascular level. In this study, we detected three enhancement patterns among the 56 patients with TIMI grade 3 flow; the variability in enhancement pattern indicates that there is variability in the extent of microvascular damage. The least extensive recovery of left ventricular function was observed in patients who had both an early and a residual perfusion defect, namely, those in group 3. That is, they might not have complete reperfusion at the microvascular level, while those patients who did not have an early or a residual perfusion defect (group 1) might experience a complete recovery of left ventricular function, which might be

indicative of successful reperfusion at both the epicardial and the microvascular level.

Importance of an Early Defect

Contrast medium is thought to reach the microvascular bed in the early phase after intravenous administration. A study involving electron-beam CT (16) revealed that myocardial enhancement in the early phase reflected the volume of the vascular bed.

Reduced signal intensity on first-pass contrast-enhanced MR images has been shown to indicate reduced blood flow (28). Therefore, an early perfusion defect observed by using CT would also reflect a decrease in the volume of the vascular bed—that is, a decrease in the myocardial blood flow.

Using an experimental infarct-reperfusion model in dogs, Braunwald and Kloner (29) classified the condition of myocardial tissue into four layers beginning from the endocardial side. The first layer corresponded to a viable and very thin myocardium that received oxygen directly from the left ventricle; the second layer, to myocardial necrosis with extensive capillary (microcirculation) disorder; the third layer, to myocardial necrosis in which blood supply was preserved to some extent; and the fourth layer, to stunned myocardium that had escaped necrosis. The early perfusion defect in our study may correspond to the second and third layers—that is, to tissue with moderate to severe microvascular damage and myocardial necrosis—because the wall thickness in groups 2 and 3 had significantly decreased. In particular, 21 (58%) patients with a transmural early perfusion defect in group 3 developed myocardial scar formation about 12 months after reperfusion therapy. Our findings are supported by the results of an MR imaging–based study, which showed that 68% of patients with microvascular obstruction in the postinfarction period had a thinning of the ventricular wall consistent with scar formation at 6 months (30).

Importance of Residual Defect and Late Enhancement

After the contrast medium reaches the microvascular bed, it gradually flows into the interstitium (extracellular space), stays there, and is then washed out slowly. Therefore, myocardial enhancement in the late phase mainly reflects the characteristics of the interstitium—that is, the volume of the interstitial space (16). When myocardial cells are damaged and the cell number decreases after an acute MI, the volume of the interstitial space increases.

In the present study, when a residual perfusion defect was detected, as it was in group 3, functional recovery was not observed. However, when an early perfusion defect turned into late enhancement, as happened in group 2, deterioration of left ventricular function was minimal or less than that observed in group 3. We speculate that the area of residual perfusion defect might correspond to the second layer (myocardial necrosis with extensive capillary disorder) of the Braunwald classification and that late enhancement might correspond to the third layer, where blood supply is preserved to some degree, indicating possible residual myocardial viability.

In this study, the percentage decrease in wall thickness in group 3 was significantly greater than that in group 2—that is, the residual perfusion defect in group 3 indicated that there was less antegrade microvascular flow beyond the point of microvascular obstruction in group 3 than in group 2. As a result of incomplete perfusion at the microvascular level, the percentage decrease in wall thickness in group 3 was greater than that in group 2 in the intermediate phase and long-term studies.

Given our results, we may conclude that a residual perfusion defect indicated a necrotic area caused by severe microvascular obstruction—the so-called no-reflow phenomenon (31) that is caused by the presence of red blood cells and necrotic debris (32) in the "wavefront" of ischemic necrosis (33,34).

In general, there is a consensus that delayed hyperenhancement at MR imaging reflects nonviable myocardium (30). However, other studies involving humans revealed that 3–5 days after a reperfused MI, some regions of enhancement recovered function 3 months later (10,35). In our study, late enhancement was also observed in both group 1 and group 2, indicating that the area of late enhancement includes viable myocardium, at least in part, at examinations performed within 48 hours of reperfusion therapy. An MR imaging–based study in rats that involved occluding the coronary artery for 30 minutes and for 2 hours revealed that the enhanced zone was time dependent (ie, it decreased in size over time), and the true infarct size corresponded to the enhancement size at 21 minutes ± 4 (36). On late images, which were acquired 7 minutes after the start of the administration of the contrast medium in that study, the true infarct size might have be overestimated; however, the contrast medium had been slowly injected at 0.1 mL/sec (to a total of 37.5 mL) after the bolus injection at 1.5 mL/sec (to a total of 112.5 mL). The total dose and injection rate of the bolus and/or the continuous injection of the contrast medium might have had an effect on the size of the enhancing lesion, although these factors were not investigated in that study.

After successful reperfusion therapy, both the wall thickness and the microvasculature change dynamically during the acute healing stage. Therefore, in the clinical setting, we assume that the timing of the CT examination after reperfusion therapy is important in assessing late enhancement with contrast-enhanced CT.

However, this concept of these enhancement patterns and their combinations at CT has not attained wide acceptance, and because CT can also help define the depth and extent of early and residual perfusion defects and late enhancement, the sizes of these parameters in comparison with the infarct size should be investigated in future studies.

Study Limitations

In this study, because the images were read concurrently by four observers and we could not compare interobserver and intraobserver agreement, interobserver and intraobserver reliabilities were not confirmed.

Regarding the x-ray exposures during two-phase contrast-enhanced CT, the radiation dose for one acquisition was 9.4 mGy. In our protocol, we performed three two-phase contrast CT studies, for a radiation dose of 18.8 mGy for each study and a total of 56.4 mGy, which does not include the fluoroscopy dose at angioplasty and angiography. Although x-ray exposure dose was high in this study, our results suggest that if two-phase contrast-enhanced helical CT was performed once within 48 hours after reperfusion therapy, the enhancement patterns could be evaluated and these enhancement patterns would serve to predict left ventricular function and wall thickness, while the x-ray exposure at this examination would be 18.8 mGy—exactly the same exposure incurred when nonoverlapping reconstructions are used. Additionally, the exposed range (12 cm) for a two-phase cardiac CT examination is smaller than that for a three-phase abdominal CT examina-

tion. Therefore, when one considers the useful information obtained from the myocardial studies, the radiation dose seems to be acceptable for patients with heart disease that may threaten their lives.

In conclusion, in patients with acute MI, the myocardial enhancement pattern at two-phase contrast-enhanced CT performed after reperfusion therapy can serve as a predictor of left ventricular functional recovery and wall thickness.

Acknowledgments: We are grateful to Tsuyoshi Matsunaka, MD, Kazuhisa Nishimura, MD, Katsuji Inoue, MD, Kana Sakamoto, MD, and Junko Kato, MD, for their excellent assistance in data analysis. We are very grateful to Yoshiyasu Kubota (Toward, Tokyo, Japan) for technical support in data computing and to GE Yokogawa Medical Systems for analyzing and calculating the weighted CT dose index in this study.

References

1. Mochizuki T, Murase K, Higashino H, et al. Two- and three-dimensional CT ventriculography: a new application of helical CT. AJR Am J Roentgenol 2000; 174:203–208.
2. Koyama Y, Matsuoka H, Higasino H, et al. Four-dimensional cardiac image by helical computed tomography. Circulation 1999; 100: e61–e62. http://circ.ahajournals.org/cgi/content/full/100/15/e61. Accessed March 21, 2005.
3. Kachelriess M, Sennst DA, Maxlmoser W, Kalender WA. Kymogram detection and kymogram-correlated image reconstruction from subsecond spiral computed tomography scans of the heart. Med Phys 2002; 29: 1489–1503.
4. Nieman K, Oudkerk M, Rensing BJ, et al. Coronary angiography with multi-slice computed tomography. Lancet 2001; 357:599–603.
5. Achenbach S, Ulzheimer S, Baum U, et al. Noninvasive coronary angiography by retrospectively ECG-gated multislice spiral CT. Circulation 2000; 102:2823–2828.
6. Becker CR, Ohnesorge BM, Schoepf UJ, Reiser MF. Current development of cardiac imaging with multidetector-row CT. Eur J Radiol 2000; 36:97–103.
7. Abe M, Kazatani Y, Fukuda H, Tatsuno H, Habara H, Shinbata H. Left ventricular volumes, ejection fraction, and regional wall motion calculated with gated technetium-99m tetrofosmin SPECT in reperfused acute myocardial infarction at super-acute phase: comparison with left ventriculography. J Nucl Cardiol 2000; 7:569–574.
8. Watanabe K, Sekiya M, Ikeda S, Miyagawa M, Kinoshita M, Kumano S. Comparison of adenosine triphosphate and dipyridamole in diagnosis by thallium-201 myocardial scintigraphy. J Nucl Med 1997; 38:577–581.
9. Al-Saadi N, Nagel E, Gross M, et al. Noninvasive detection of myocardial ischemia from perfusion reserve based on cardiovascular magnetic resonance. Circulation 2000; 101: 1379–1383.
10. Rogers WJ Jr, Kramer CM, Geskin G, et al. Early contrast-enhanced MRI predicts late functional recovery after reperfused myocardial infarction. Circulation 1999; 99:744–750.
11. Kim RJ, Fieno DS, Parrish TB, et al. Relationship of MRI delayed contrast enhancement to irreversible injury, infarct age, and contractile function. Circulation 1999; 100:1992–2002.
12. Kim RJ, Wu E, Rafael A, et al. The use of contrast-enhanced magnetic resonance imaging to identify reversible myocardial dysfunction. N Engl J Med 2000; 343:1445–1453.
13. Bogaert J, Maes A, Van de Werf F, et al. Functional recovery of subepicardial myocardial tissue in transmural myocardial infarction after successful reperfusion: an important contribution to the improvement of regional and global left ventricular function. Circulation 1999; 99:36–43.
14. Ito H, Tomooka T, Sakai N, et al. Lack of myocardial perfusion immediately after successful thrombolysis: a predictor of poor recovery of left ventricular function in anterior myocardial infarction. Circulation 1992; 85: 1699–1705.
15. Lepper W, Hoffmann R, Kamp O, et al. Assessment of myocardial reperfusion by intravenous myocardial contrast echocardiography and coronary flow reserve after primary percutaneous transluminal coronary angioplasty [correction of angiography] in patients with acute myocardial infarction. Circulation 2000; 101:2368–2374. [Published correction appears in Circulation 2000; 102: 482.]
16. Naito H, Saito H, Ohta M, Takamiya M. Significance of ultrafast computed tomography in cardiac imaging: usefulness in assessment of myocardial characteristics and cardiac function. Jpn Circ J 1990; 54:322–327.
17. Mochizuki T, Murase K, Higashino H, Koyama Y, Azemoto S, Ikezoe J. Images in cardiovascular medicine: demonstration of acute myocardial infarction by subsecond spiral computed tomography—early defect and delayed enhancement. Circulation 1999; 99:2058–2059.
18. International Electrotechnical Commission. Medical electrical equipment: part 2–44—particular requirements for the safety of x-ray equipment for computed tomography. Document no. IEC 60601-2-44. Geneva, Switzerland: International Electrotechnical Commission, 2002; 1–36.
19. Baer FM, Voth E, Schneider CA, Theissen P, Schicha H, Sechtem U. Comparison of low-dose dobutamine-gradient-echo magnetic resonance imaging and positron emission tomography with [18F]fluorodeoxyglucose in patients with chronic coronary artery disease: a functional and morphological approach to the detection of residual myocardial viability. Circulation 1995; 91:1006–1015.
20. Dodge HT, Sandler H, Ballew DW, Lord JD. The use of biplane angiocardiography for the measurement of left ventricular volume in man. Am Heart J 1960; 60:762–776.
21. The Thrombolysis in Myocardial Infarction (TIMI) trial: phase I findings. TIMI Study Group. N Engl J Med 1985; 312:932–936.
22. The effects of tissue plasminogen activator, streptokinase, or both on coronary-artery patency, ventricular function, and survival after acute myocardial infarction. The GUSTO Angiographic Investigators. N Engl J Med 1993; 329:1615–1622.
23. Van de Werf F. Discrepancies between the effects of coronary reperfusion on survival and left ventricular function. Lancet 1989; 1:1367–1369.
24. Vogt A, von Essen R, Tebbe U, Feuerer W, Appel KF, Neuhaus KL. Impact of early perfusion status of the infarct-related artery on short-term mortality after thrombolysis for acute myocardial infarction: retrospective analysis of four German multicenter studies. J Am Coll Cardiol 1993; 21:1391–1395.
25. Karagounis L, Sorensen SG, Menlove RL, Moreno F, Anderson JL. Does thrombolysis in myocardial infarction (TIMI) perfusion grade 2 represent a mostly patent artery or a mostly occluded artery? enzymatic and electrocardiographic evidence from the TEAM-2 study. Second Multicenter Thrombolysis Trial of Eminase in Acute Myocardial Infarction. J Am Coll Cardiol 1992; 19:1–10.
26. Anderson JL, Karagounis LA, Becker LC, Sorensen SG, Menlove RL. TIMI perfusion grade 3 but not grade 2 results in improved outcome after thrombolysis for myocardial infarction: ventriculographic, enzymatic, and electrocardiographic evidence from the TEAM-3 Study. Circulation 1993; 87:1829–1839.
27. Gibson CM, Cannon CP, Murphy SA, et al. Relationship of TIMI myocardial perfusion grade to mortality after administration of thrombolytic drugs. Circulation 2000; 101: 125–130.
28. Rochitte CE, Lima JA, Bluemke DA, et al. Magnitude and time course of microvascular obstruction and tissue injury after acute myocardial infarction. Circulation 1998; 98: 1006–1014.
29. Braunwald E, Kloner RA. Myocardial reperfusion: a double-edged sword? J Clin Invest 1985; 76:1713–1719.
30. Wu KC, Zerhouni EA, Judd RM, et al. Prognostic significance of microvascular obstruction by magnetic resonance imaging in patients with acute myocardial infarction. Circulation 1998; 97:765–772.
31. Kloner RA, Ganote CE, Jennings RB. The "no-reflow" phenomenon after temporary coronary occlusion in the dog. J Clin Invest 1974; 54:1496–1508.
32. Engler RL, Schmid-Schonbein GW, Pavelec RS. Leukocyte capillary plugging in myocardial ischemia and reperfusion in the dog. Am J Pathol 1983; 111:98–111.
33. Reimer KA, Lowe JE, Rasmussen MM, Jennings RB. The wavefront phenomenon of ischemic cell death. I. Myocardial infarct size vs duration of coronary occlusion in dogs. Circulation 1977; 56:786–794.
34. Reimer KA, Jennings RB. The "wavefront phenomenon" of myocardial ischemic cell death. II. Transmural progression of necrosis within the framework of ischemic bed size (myocardium at risk) and collateral flow. Lab Invest 1979; 40:633–644.
35. Kramer CM, Rogers WJ Jr, Mankad S, Theobald TM, Pakstis DL, Hu YL. Contractile reserve and contrast uptake pattern by magnetic resonance imaging and functional recovery after reperfused myocardial infarction. J Am Coll Cardiol 2000; 36:1835–1840.
36. Oshinski JN, Yang Z, Jones JR, et al. Imaging time after Gd-DTPA injection is critical in using delayed enhancement to determine infarct size accurately with magnetic resonance imaging. Circulation 2001; 104:2838–2842.

一般演題14

車載型らせんCTを用いた胸部検診における経過観察例のCT所見

潤間隆宏[*1]　鈴木公典[*2]　大平尚子[*2]　佐藤由梨[*2]
小野崎郁史[*2]　長尾啓一[*3]　猪狩英俊[*4]　天野佳子[*5]
渡辺哲[*5]　滝口裕一[*5]　栗山喬之[*5]

[目的]車載型らせんCTを用いた胸部検診において、経過観察と判定された群と、肺癌・異型腺腫様過形成と確定診断された群との間でthin-section CT所見の比較検討をおこなった。
[対象と方法]一自治体住民849名を対象として、車載型らせんCTを用いた一次検診を行なった。精密検査が必要と判定された例にthin-section CTを施行し、確定診断が必要な例は精査医療機関受診を推奨した。
[結果]要精査100例中83名に、精査CTを撮像した。CTガイド下生検・胸腔鏡下肺生検・開胸肺生検などの診断的検査により肺癌5例、AAH1例が診断された。2年間の経過観察継続および終了例は18例であった。経過観察継続例で他部位の陰影出現と消失が1例に、陰影の増大が1例に認められた。肺癌・AAH6名6病変のC群と経過観察継続・終了群18名22病変につき、thin-section CT所見の比較検討を行い、辺縁不整・辺縁不鮮明・内部のすりガラス濃度・air bronchogram・静脈関与が、各群間において所見の比率に有意な差がみられた。
[結論]辺縁不整・辺縁不鮮明・すりガラス濃度・air bronchogram・静脈関与の所見が悪性病変を示唆する所見と考えられた。
キーワード：　車載型らせんCT、thin-section CT、肺癌、経過観察、胸部検診

はじめに

低線量CTを用いた胸部検診により、より小さなそしてより早期の肺癌を発見することが可能になり、肺癌死亡率の低下への寄与が期待されている。しかし、検出した肺野結節は、thin-section CT所見でも良悪性の鑑別が難しく経過観察を行う例も多い。今回我々は、車載型らせんCTを用いた胸部検診において精査CTで経過観察と判定された例と、肺癌・異型腺腫様過形成と確定診断された例のthin-section CT所見の比較検討をおこなった。

[*1]千葉県立東金病院
(〒283-8588　千葉県東金市台方1229)
e-mail:uruma-t@umin.ac.jp
[*2]ちば県民保健予防財団
[*3]千葉大学総合安全衛生管理機構
[*4]千葉大学医学部附属病院感染症管理治療部
[*5]千葉大学医学研究院加齢呼吸器病態制御学

方法

2001年度に、千葉県内一自治体住民849名を対象として、ちば県民保健予防財団が、車載型らせんCTを用いた一次検診を行った。CT装置は、日立メディコ社製CT-W950SRを用い、撮像条件は、120 kV, 50mA, スライス幅10 mm, テーブル移動速度20 mm/sec, 2秒/回転であった。読影は、比較読影支援システムを用いてCRT上で用い、一症例につき2名の読影医が独立して読影を行った。2名の読影医のうち、いずれか1名以上が要精査とした症例について、合同判定を施行し、B判定(異常なし)C判定(異常所見を認めるが精査を必要としない)、D1判定(活動性肺結核を強く疑う)、